https://doi.org/10.2352/ISSN.2470-1173.2017.17.COIMG-419

A Randomized Approach to Reduce Metal Artifacts in X-Ray Computed Tomography

Parisa Babaheidarian and David Castañón; Boston University; Boston, MA/U.S.A.

Abstract

We introduce a new algorithm to reduce metal artifacts in computed tomography images when data is acquired using a single source spectrum. Our algorithm is a hybrid approach which corrects the sinogram vector followed by an iterative reconstruction. Many prior sinogram correction algorithms identify projection measurements that travel through areas with significant metal content, and remove those projections, interpolating their values for use in subsequent reconstruction. In contrast, our algorithm retains the information of random subsets of these metal-affected projection measurements, and uses an average procedure to construct a modified sinogram. To reduce the secondary artifacts created by this interpolation, we apply an iterative reconstruction in which the solution is regularized using a sparsifying transform. We evaluate our algorithm on simulated data as well as data collected using a medical scanner. Our experiments indicate that our algorithm reduces the extent of metal artifacts significantly, and enables accurate recovery of structures in proximity to metal.

Introduction

Most scanners used in Computed Tomography (CT) applications use x-ray sources that generate photons based on Bremsstrahlung radiation, thereby resulting in source spectra that span a broad range of energies. Since the attenuation properties of different materials are energy dependent, the spectral mixture of photon energies changes as the x-rays penetrate through different materials. In particular, the presence of denser materials with higher attenuation such as metals can lead to significant spectral distortion through absorption of low-energy photons. Most reconstruction algorithms fail to account for such distortions in their processing, resulting in the presence of significant artifacts in the reconstructed images. Further artifacts are introduced through improper modeling of photon scatter, partial volume effects in the discretizations used for image reconstruction, and noisy signals due to photon starvation and errors in data sampling [1].

In medical imaging, metal is not a normal part of most anatomies, so metal artifact arise in areas where external metal has been introduced. When metal is present, it causes streaks and shadows that obscure surrounding tissue, making it difficult for radiologists to evaluate images. In security imaging, the presence of metal in luggage is ubiquitous, and can recreate significant artifacts, such as shadows or bright streaks and blurring, that interfere with the task of object segmentation and recognition. These artifacts can lead to splitting or merging of objects, and result either in missed detection of important objects or false alarms.

There has been significant prior work to reduce the presence of metal artifacts in CT images [2–10] motivated by different applications. The most common approach is based on sinogram replacement through interpolation. Examples of sinogram interpolation schemes are the linear interpolation (LI) algorithm [3] and the metal deletion technique (MDT) [4]. Both of these approaches have been effective in removing metal artifacts in medical imagery [4] when there is minimal amounts of metal present. These methods start from a reconstructed image using filtered back projection (FBP), and identify locations of high attenuation, defining this as the metal region. They subsequently identify projection measurements that pass through the metal region, and seek to modify these measurements. In the LI method, the values of these metal-passing projection measurements are linearly interpolated using the adjacent projections that did not overlap the metal region. The MDT method performs a more complicated iterative correction: The first step is to perform the interpolation using an LI approach; in subsequent iterations, it reconstructs the image and does further modifications to the sinograms in order to generate a reconstructed image without the presence of metal. A different approach to sinogram interpolation was proposed in [5], where sparse wavelet interpolation was used to generate estimates of the projection measurements that pass through the metal region.

One of the main limitations of these sinogram interpolation techniques is that they discard the information of projection measurements that overlap the metal region, and thus lose a lot of information about areas in proximity to metal regions or surrounded by metal. This can lose critical information in security imaging, leading to inability to detect objects in metal enclosures or adjacent to significant metal structures. Furthermore, the sinogram manipulations often result in introduction of secondary artifacts in the reconstruction. More sophisticated techniques for sinogram interpolation use iterative reconstruction together with removal of projections that intersect the metal region, as in [2].

Another class of metal artifact reduction technique are based on image domain approaches, and aim to correct the image by modifying the areas affected by metal. Examples of such methods are image in-painting approaches, coupled with different methods of iterative reconstruction of the original sinogram [6–8]. In [6], Jin et al. proposed a metal artifact reduction method in which regions in the image affected by metal were identified, and then interpolated using an image in-painting technique. in [9, 10], the authors used the identified metal region, along with iterative reconstruction techniques, to compute estimates of the artifacts in the image, which they then subtracted from the original image.

In this paper, we introduce a hybrid approach to reduce metal

This material is based upon work supported by the U.S. Department of Homeland Security, Science and Technology Directorate, Office of University Programs, under Grant Award 2013-ST-061-ED0001. The views and conclusions contained in this document are those of the authors and should not be interpreted as necessarily representing the official policies, either expressed or implied, of the U.S. Department of Homeland Security.

artifacts in CT images when the data is acquired using a single source spectrum. To reduce the chance of information loss, we utilize the information of both metal-passing and non-metal passing projection measurements to generate an interpolated sinogram. The sinogram correction is performed through several iterations: at each iteration, a random subset of metal-passing projection measurements is selected to be corrected and the value of other projection measurements are kept fixed as in their original values. To correct the selected subset, sinogram values are interpolated in wavelet domain as in [5]. This process is repeated several times and each time we obtain a new sinogram vector. Our final sinogram is the average over the corrected sinogram vectors. In the next step, we reconstruct the image from the average corrected sinogram. We choose an iterative reconstruction with the motive of removing secondary artifacts that are the by-products of sinogram manipulation in the previous step. To this end, we learn a sparsifying transform from the patches of the original FBP image which does not contain the secondary artifacts, then we use this transform as a regularization term for the iterative image reconstruction.

We evaluate our algorithms on data generated through simulations, as well as data collected from a medical scanner. Our experiments show that our algorithm effectively reduces the metal artifacts and reconstructs the attenuation properties of materials near metal accurately, whereas alternative algorithms fail to accomplish.

In the following sections, we explain the steps of our algorithm in details. Then, we present our experiments and evaluate the performance of our algorithm, followed by a comparison against recent methods suggested for reduction of metal artifacts in CT. Our conclusion section discusses our results, and indicates directions for future work.

Our algorithm

We propose a new hybrid algorithm in which we correct the metal passing projection measurements in the sinogram domain followed by an iterative reconstruction. Unlike previous algorithms in [3], [4], and [5] that discard information from metal-passing projection measurements, we will use this information as well as the information in non-metal passing projection measurements in order to reduce the chance of information loss in correcting the sinogram. We describe our algorithm in three steps below: sinogram correction, learning a sparsifying transform, and iterative reconstruction.

Sinogram correction

Our algorithm starts from an FBP image obtained using a filtered backprojection algorithm (FBP). We detect any pixels where the estimated attenuation coefficient exceeds a threshold Th to obtain a set of pixels M which we refer to as a metal mask. Typically, this threshold is selected in the range from 3000 to 4000 in MHU.[1]

Our next step is to identify projection measurements in the sinogram where the projections intersect the metal mask M. These projection measurements in the sinogram are identified as $\mathbf{Y}_M$, the set of measurements that are affected by metal. The remaining projection measurements in the sinogram represent the set of measurements not affected by metal, and are denoted as the complement set Y_{M^c}. Therefore, we have:

$$Y = Y_M \cup Y_{M^c}, \tag{1}$$

where Y is the complete set of projection measurements, the sinogram matrix.

Our goal is to generate a set of corrected measurements $\tilde{Y}_M$. To do so, we perform the following steps in an iterative manner:

1. Initialize $\tilde{y}_k = 0$ for all measurements k.
2. For each iteration in 1 to N_s:
   (a) Select a random subset $S \subset M$.
   (b) Interpolate values in the set S as the solution to the following constrained minimization problem:
   $$Y^{(i)} \triangleq \arg\min_{\hat{Y}} \|W\hat{Y}\|_1 \tag{2}$$
   such that
   $$\hat{Y}_{S^c} = Y_{S^c} \tag{3}$$
   (c) Set $\tilde{y}_k = \tilde{y}_k + \hat{y}_k^{(i)}$ for all measurements k
3. Compute the average sinogram Y^{avg} as
   $$y_k^{avg} \triangleq \frac{1}{N_s}\tilde{y}_k \text{ for all pixels } k \tag{4}$$

In (2), W is a 2D wavelet transform operator[2] and $\|.\|_1$ is the ℓ_1-norm which is applied to the wavelet coefficients in the vector form. Also, in (3), set S^c is the complement set of set S in the set of all measurements; this constraint ensures that all values in S^c are fixed and are equal to the values of the original sinogram at those indices. Note that the values of non-metal passing rays in set M^c in Y^{avg} will be the same as in the original sinogram Y, due to the constraint in (3). The constrained optimization in (2) was solved using majorization-minimization technique and projected gradient descent [5].

The intuition behind using wavelet interpolation in (2) is to reduce high-frequency details and noise by imposing sparsity constraint on the corresponding wavelet coefficients. A similar idea was also used in [5]; however, they used the wavelet interpolation to update all the metal-passing rays at the same time which led to loss of information regarding the structures near metal in the reconstructed image.

Learning a sparsifying transform

In this step, we construct the ingredients of the regularization term which will be used in the iterative reconstruction. We observed that FBP reconstruction of interpolated sinograms suffers from secondary artifacts. This phenomenon is common to most algorithms which modify the original sinogram [3–5]. The secondary artifacts do not exist in the original FBP image and are by-products of the sinogram processing. Therefore, in our algorithm, we learn a sparsifying transform [11] from the patches of the original FBP image as in the following:

$$\min_{T,\{\mathbf{z}_j\}_j} \|TX^{FBP} - Z\|_F^2, \ \ \|\mathbf{z}_j\|_1 \le q \ \forall j \tag{5}$$

[1] MHU is the HU unit with offset in which linear attenuation of water is 1000: $\mu_{MHU} = \frac{\mu}{\mu_{water}} \times 10^3$.

[2] We used JPEG-2000 in our experiments.

In (5), T is an over-complete sparsifying transform, $\|.\|_F^2$ represents the Frobenius norm, X^{FBP} is the matrix of overlapping patches of the original FBP image, patches are of size $\sqrt{K} \times \sqrt{K}$ for some K and T is of size $2K \times K$. Vector $\mathbf{z}_j$ is the sparse code for patch j, Z is the matrix of sparse codes for all patches, and q is the sparsity level which is a parameter of the problem.

The optimization in (5) finds a transform T which maps the patches of the original FBP image to sparse vectors. We solved this optimization problem as in [11], using an iterative algorithm solving for T and for Z respectively. Sparsifying transforms were used in [11] for image de-noising; in our application, we use it to learn the transform basis T that should make our reconstruction sparse.

Iterative reconstruction

In the final step of our algorithm, an image estimate is reconstructed using an iterative reconstruction algorithm . We work with the corrected sinogram vector $Y^{avg} \equiv \mathbf{y}_{avg}$. We assume a linear model between image vector and sinogram vector, i.e., $\mathbf{y} = A\mathbf{x}$, and use the learned sparsifying transform to regularize the solution. We cast the image reconstruction problem as:

$$\min_{\mathbf{x},\{\mathbf{z}_j\}_j} \|\mathbf{y}_{avg} - A\mathbf{x}\|_D^2 + \lambda \sum_{j=1}^{(N-\sqrt{K}+1)^2} \|TE_j\mathbf{x} - \mathbf{z}_j\|_2^2 \tag{6}$$

such that

$$\|\mathbf{z}_j\|_1 \leq q \ \ \forall j \tag{7}$$

Matrix A in (6) is the forward projection matrix (the system matrix), matrix D is the weighting matrix to down-weight the Poisson noise, which is a diagonal matrix with its i-th element as

$$D(i,i) = e^{-c\mathbf{y}_{avg}(i)}, \ \ c \geq 1 \tag{8}$$

Also, E_j is the patch extractor matrix for patch j, patches are of size $\sqrt{K} \times \sqrt{K}$ and are over-lapping and the image vector $\mathbf{x}$ is of size $N^2 \times 1$.

The regularization term in (6) together with constraint (7) encourages the patches of the image estimate to be sparse in the domain of transform T. By doing so, the amount of secondary artifacts in the reconstructed image are reduced since transform T was learned from the original FBP image in which no secondary artifacts exist. The parameter λ balances the cost between fitting the image to the corrected sinogram and the cost of sparsifying transform.

The constrained minimization problem in (6) is convex. We used the alternating direction method of multipliers (ADMM) [13], which enables us to use separate the minimization of $\mathbf{x}$ in the data fidelity term from that of the regularization term, leading to a simple iterative algorithm.

Experiments

To evaluate the performance of our algorithm versus alternative approaches, we developed simulated 2-D data sets based on variations of the FORBILD head phantom [12]. We added metal and other materials in different locations, the materials included are bone, air, steel and ethanol. In our phantoms, ethanol regions are surrounded by thin steel containers, as illustrated in Fig. 1. Next,

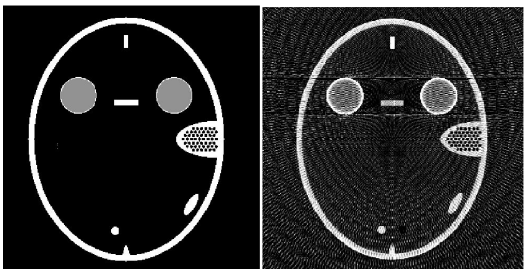

Figure 1. *The constructed FORBILD phantom with bone, air, ethanol (gray areas), and metal containers (bright circles) on the left and a sample FBP reconstruction at 130 Kvp voltage source, in [0-0.8] cm^{-1} display range.*

we simulated a polychromatic source spectrum with a source operating at 130 Kvp which is an approximation to the Imatron C300 scanner spectral weighting [7]. We sampled the spectrum at 40 energy levels to get the discrete normalized energy weight $W(.)$. The initial flux was considered as $I_0 = 3 \times 10^4$. We simulated the sinogram using 150 projections evenly spaced from 0 to 180 degrees and 100 detectors per projection. The linear attenuation coefficients of the different materials were obtained from the NIST XCOM database [14].

The received photon counts at a detector were simulated as a Poisson random variable. Letting L_i denote the projection path to detector i, we have

$$c_i = \text{Poi}\left(\sum_{j=1}^{40} I_0 W(j) e^{-\int_{L_i} \mu(\vec{r},j)d\ell}\right) \tag{9}$$

where c_i are the simulated photon counts measured by detector i, $\mu(\vec{r},j)$ is the linear attenuation coefficient at energy level j and is a function of the energy j at spatial location $\vec{r}$. The line integral $\int_{L_i} \mu(\vec{r},j)d\ell$, along the projection path L_i at energy level j, was computed using the software tools in [12].

The sinogram values we use for the detectors are measured in log scale, as

$$y_i = -\log\left(\frac{c_i}{I_0}\right) \tag{10}$$

We reconstructed the images from the simulated sinograms using filtered backprojection (FBP). An original image and the reconstructed image are shown in Fig. 1. Note the presence of circular ringing artifacts and additional streaks introduced by the presence of the two steel circles.

To compare the performance of our algorithm, we implemented several other metal artifact reduction techniques: the LI interpolation technique of [3], the MDT algorithm of [4], the image in-painting technique of [6], and the artifact subtraction technique of [10]. We tested each of these algorithms, as well as our algorithm, to reconstruct the image illustrated in Fig. 1. The final reconstructions provided by the different algorithms are shown in Fig. 2.

Examining the reconstructions in Fig. 2, the simple LI algorithm does a good job of reducing the metal artifacts. However, it also deletes all information in the ethanol region, reconstructing it as air. This is a consequence of discarding all of the information

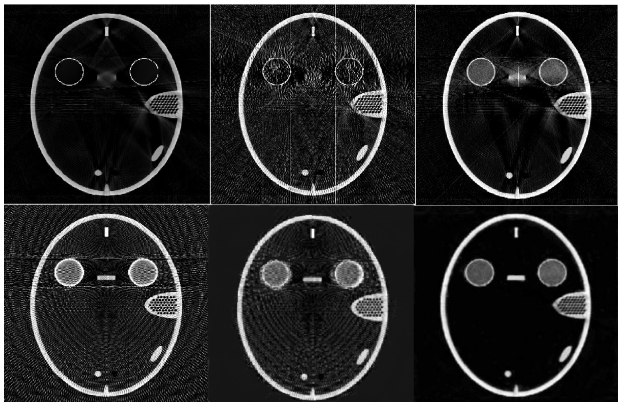

Figure 2. *Performance comparison on FORBILD phantom, in [0-0.8] cm^{-1} display range: the top row, from left to right: LI [3], MDT [4], and FBP reconstruction of the average corrected sinogram in our algorithm. The bottom row, from left to right: An image in-painting method [6], a hybrid approach [10], and our algorithm's final image.*

in measurement projections that include metal in the projection path. The more complex MDT algorithm also reduces the original metal artifacts, but creates a number of secondary artifacts in its iterations. It also deletes all information concerning the ethanol region in the two steel enclosures.

The image in-painting technique of [6] and the artifact subtraction technique of [10] are able to preserve information as to the presence of some material inside of the steel circles. However, the in-painting technique does not reduce the original artifacts much, because many of the artifacts are not shaped like streaks. The images on the right side of Fig. 2 correspond to two variations of our algorithm. The top image is the filtered backprojection reconstruction of our modified sinogram, and the bottom image is the iterative reconstruction algorithm described previously. Note that the FBP image has reduced the original artifacts significantly, but there are some secondary artifacts introduced, as evidenced in the blurring near the metal circles. Our full algorithm with iterative reconstruction reduces these secondary artifacts.

Even though the algorithms of [6, 10] preserved the presence of material inside of the steel cylinders, the resulting reconstructed values were inaccurate. To determine the appropriate reconstructed value for the ethanol region, we created a new phantom where the metal containers were removed, and performed an FBP reconstruction using the new data. We computed the mean and variance of the reconstructed linear attenuation coefficient in the ethanol region for this new phantom, and considered that as the "ground truth" that the algorithms should estimate when the metal cylinders are present. Subsequently, we computed the mean and variance of the reconstructed linear attenuation coefficient in the regions inside of the metal cylinders for each of the reconstructions shown in Fig. 2.

Table 1 displays the results of this analysis. Due to metal artifacts, the original FBP reconstruction overestimates the attenuation inside of the metal cylinders significantly. Interestingly, the algorithms of [6, 10] improve minimally on this estimate, and continue to overestimate the attenuation in the region enclosed by

	Mean	Variance
FBP no metal container	0.2512	0.0015
FBP with metal container	0.5543	0.7559
Our algorithm	0.2763	0.008
MDT [4]	0.0819	0.8603
LI [3]	0.0406	0.00025
Alternative 3 [10]	0.5020	0.6862
Alternative 4 [6]	0.4838	0.3343

Table 1. Performance evaluation of different reconstruction methods on the FORBILD phantom with metal shields and ethanol. The mean and variance were computed in the ethanol regions.

metal by nearly a factor of 2, which would likely lead to erroneous classification of this material. As expected, the LI and MDT algorithms significantly underestimate the attenuation in this region. Our algorithm shows accurate reconstruction in the region, with small errors in mean and variance when compared to the estimates obtained from the FBP reconstruction with no metal enclosures. This suggests that our approach preserved essential information concerning the enclosed region.

We further evaluated the performance of our proposed algorithm on real data acquired by a medical scanner, the GE Imatron C300 electron-beam tomography (EBT) scanner. The data we used was collected as part of the ALERT TO3 data collection [7]. The data set consisted of different slice scans of a cluttered bag, which contained bottled water, rubber sheets, a Teflon box, metal objects, and other clutter such as clothing. The X-ray tube was driven at 130 kVP. The sinogram was generated using a re-binned collection of parallel projections, with 720 projections and 1024 detectors per projection. The reconstructed images are of size a 512×512 and are displayed in MHU units and the display range used in the figures is [0-1500] MHU.

To evaluate our algorithm's performance on this data set, we chose a slice and collected its corresponding parallel projection data. Using the original FBP image, we identified the metal region by selecting pixels with reconstructed attenuation that exceeds a threshold of 4000 MHU to the original FBP image. Using the forward projection system matrix, as estimated in [7], we identified the projections in the sinogram that intersect the metal region. The random sub-sampling and sinogram modification process was performed for $N_s = 100$ iterations. At each repetition, we selected as a random subset S to correspond to 80% of the projections that intersect the metal region. Using this approach, the average sinogram was computed as described in (4). The final images were reconstructed using the optimization in (6).

Figure 3 illustrates the metal artifact reduction performance of our algorithm, and compares it to those obtained using the methods in [3] and [4]. As it was expected, our algorithm displays an improvement in reconstructing the boundaries of metal and structures close to metal regions, and it reduces the secondary artifacts significantly. In order to make the images comparable, the value of pixels in the metal region were added to the final images in the MDT and LI reconstructions.

Figure 4 illustrates the performance of the tested algorithms on a different slice of the bag which compares our algorithm's performance against the LI method in [3]. In this reconstruction, we did not insert back the metal region values in the image gen-

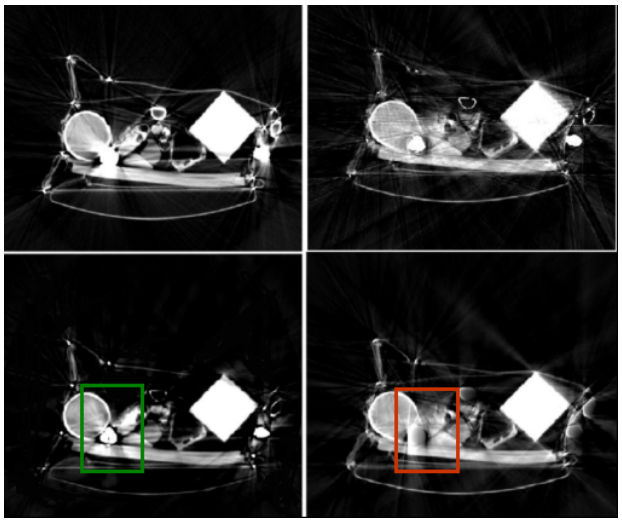

Figure 3. *Reconstructed image of a slice of a highly cluttered bag in ALERT task order 3 dataset [7] using different methods in [0-1500] MHU display range: the top-left image is the original FBP image, the top-right is the MDT image [4], the bottom-left shows our algorithm's result, and finally the bottom-right shows the LI image [3]. Our algorithm recovers the area near the metal and boundaries effectively while the tested alternatives struggle in proximity to metal and show visible secondary artifacts.*

erated by the LI algorithm. Our algorithm recovers structures that are located near metal better than the tested alternative.

Conclusion

In this paper, we introduced a new metal artifact reduction algorithm for CT images. Our algorithm is a hybrid approach which corrects projection measurements passing through metal regions, followed by an iterative reconstruction. The sinogram modification procedure uses a novel randomized sampling approach that preserves a fraction of the affected projection measurements. The iterative reconstruction approach uses a sparsified transform learned from the original filtered backprojection image in order to reduce the presence of secondary artifacts introduced by the sinogram modification.

We evaluated our algorithm, and compared its performance to several alternative metal artifact reduction approaches suggested in the literature. In limited testing using both simulated data and data from a medical scanner, our algorithm had superior performance to the alternative algorithms. In particular, the results indicate that our algorithm is able to recover structures that are surrounded by metal much more accurately than the alternative approaches.

The main limitations of our algorithm are the processing time complexity, both in the sinogram correction technique and in the iterative reconstruction algorithm. The sinogram correction technique requires the solution of multiple sparse wavelet interpolation problems. The iterative reconstruction algorithm requires learning a sparsifying transform, and subsequently using this in a sparse regularized iterative reconstruction technique.

In terms of future directions, the promising results shown in this paper need to be verified using more extensive simulation

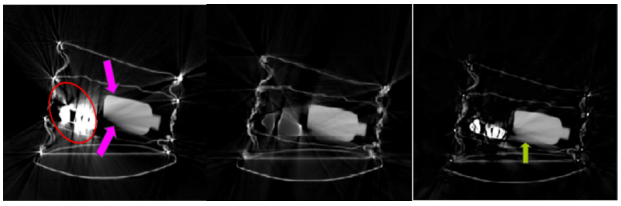

Figure 4. *Reconstructed image of another slice of a highly cluttered bag in ALERT task order 3 dataset [7] using different methods in [0-1500] MHU display range: the left image is the original FBP image, the image in the middle is the LI image [3] before superimposing metal mask, and the right image shows our algorithm's result. Our algorithm keeps the metal and recovers the structures near the metal effectively.*

and data collection. We have recently collected additional data sets on the same medical scanner with significantly more metal present, including metal enclosures. In addition, we will explore alternative algorithms that can lead to reduction in computation time.

References

[1] B. D. Man and J. Nuyts, Metal streak artifacts in X-ray computed tomography: a simulation study, Nuclear Science Symposium, pp. 1860-1865, (1998).

[2] Y. Zhang, H. Yan, X. Jia, J. Yang, S. Jiang and X. Mou, A hybrid metal artifact reduction algorithm for x-ray CT, Medical Physics, 40, (2013).

[3] Kalender, W. A., Hebel, R., and Ebersberger, J., Reduction of CT artifacts caused by metallic implants. Radiology, 164, 2, (1987).

[4] Boas, F. E., and Fleischmann, D., Evaluation of two iterative techniques for reducing metal artifacts in computed tomography, Radiology 259, 3, (2011).

[5] Mehranian, A., M. R. Ay, A. Rahmim, and H. Zaidi, Sparsity constrained sinogram inpainting for metal artifact reduction in x-ray computed tomography, IEEE Nuclear Science Symposium and Medical Imaging Conference (NSS/MIC), pp. 3694-3699, (2011).

[6] C. Crawford, Advances in automatic target recognition (ATR) for CT based object detection system–Final report, Dept. Homeland Security Center Excellence, Task order number HSHQDC-12-J-00429, Boston, MA, (2014).

[7] C. Crawford, H. Martz, and W. C. Karl, Research and development of reconstruction advances in CT-based object detection systems–Final report, Dept. Homeland Security Center Excellence, ALERT, Boston, MA, Tech. Rep. HSHQDC-12-J-00056, (2013).

[8] Jin, P., Ye, D. H., and Bouman, C. A., Joint metal artifact reduction and segmentation of ct images using dictionary-based image prior and continuous-relaxed potts model, IEEE Image Processing (ICIP),(2015).

[9] Do, S., and Karl, W. C., Sinogram sparsified metal artifact reduction technology (SSMART), The third international conference on image formation in X-ray computed tomography, (2014).

[10] Karimi, S., Cosman P., and Martz H., Metal artifact reduction for CT-based luggage screening, IEEE International Conference on Acoustics, Speech and Signal Processing (ICASSP), (2014).

[11] Ravishankar, S., and Bresler, Y., Learning sparsifying transforms, IEEE Transactions on Signal Processing, 61, 5, (2013).

[12] Yu, Z., Noo, F., Dennerlein, F., Wunderlich, A., Lauritsch, G., and

Hornegger, J., Simulation tools for two-dimensional experiments in x-ray computed tomography using the FORBILD head phantom, Physics in medicine and biology, 57, 13, (2012).

[13] Boyd, S., Parikh, N., Chu, E., Peleato, B. and Eckstein, J., Distributed optimization and statistical learning via the alternating direction method of multipliers. Foundations and Trends in Machine Learning. 3, 1 (2011).

[14] M. Berger et al, XCOM: Photon Cross Sections Database, Available online: http://physics.nist.gov/xcom (2005).

Author Biography

Parisa Babaheidarian received the B.Sc. degree in electrical engineering from University of Tehran in 2008. She graduated with the M.Sc. degree in electrical engineering from Sharif University of Technology in 2011. Currently, she is a Ph.D. candidate in electrical engineering program at Boston University. Her research interests include image recognition, analyzing CT images, signal processing, machine learning, and information theory.

David Castañón is Professor of Electrical and Computer Engineering at Boston University. He received his Ph.D. in Applied Mathematics from MIT (1976). He was Chief Scientist at ALPHATECH before joining Boston University (1990). He has been ECE Department Chair, co-director of the Center for Information and Systems Engineering, President of the IEEE Control Systems Society, and member of Air Force's Scientific Advisory Board. His interests include control, estimation, optimization, inverse problems and image understanding.